PCCP

Cite this: *Phys. Chem. Chem. Phys.*, 2011, **13**, 10699–10708

www.rsc.org/pccp

PAPER

HO_2 formation from the OH + benzene reaction in the presence of O_2

Sascha Nehr, Birger Bohn,* Hendrik Fuchs, Andreas Hofzumahaus and Andreas Wahner

Received 8th February 2011, Accepted 5th April 2011
DOI: 10.1039/c1cp20334g

In this study we investigated the secondary formation of HO_2 following the benzene + OH reaction in N_2 with variable O_2 content at atmospheric pressure and room temperature in the absence of NO. After pulsed formation of OH, HO_x (= OH + HO_2) and OH decay curves were measured by means of a laser-induced fluorescence technique (LIF). In synthetic air the total HO_2 yield was determined to be 0.69 ± 0.10 by comparison to results obtained with CO as a reference compound. HO_2 is expected to be a direct product of the reaction of the intermediately formed OH–benzene adduct with O_2. The HO_2 yield is slightly greater than the currently recommended yield of the proposed HO_2 co-product phenol (~53%). This hints towards other, minor HO_2 forming channels in the absence of NO, *e.g.* the formation of epoxide species that was proposed in the literature. For other test compounds upper limits of HO_2 yields of 0.10 (isoprene) and 0.05 (cyclohexane) were obtained, respectively. In further experiments at low O_2 concentrations (0.06–0.14% in N_2) rate constants of (2.4 ± 1.1) × 10^{-16} cm^3 s^{-1} and (5.6 ± 1.1) × 10^{-12} cm^3 s^{-1} were estimated for the OH–benzene adduct reactions with O_2 and O_3, respectively. The rate constant of the unimolecular dissociation of the adduct back to benzene + OH was determined to be (3.9 ± 1.3) s^{-1}. The HO_2 yield at low O_2 was similar to that found in synthetic air, independent of O_2 and O_3 concentrations indicating comparable HO_2 yields for the adduct + O_2 and adduct + O_3 reactions.

1. Introduction

In the troposphere the OH-initiated photo-oxidation of aromatic hydrocarbons results in the formation of ozone and secondary organic aerosol. Therefore, aromatic compounds are important pollutants with regard to air quality.[1,2]

Benzene is among the most abundant aromatic trace constituents of the atmosphere originating mainly from anthropogenic sources including evaporative emissions of chemical plants and storage tanks as well as incomplete combustion processes.[3] Owing to its atmospheric lifetime of several days, benzene can undergo long-range transport after emission in urban areas and thus impacts regional air pollution levels. Under atmospheric conditions benzene reacts predominantly with the OH radical. The benzene + OH reaction proceeds *via* reversible addition to the aromatic ring yielding the hydroxycyclohexadienyl radical (Fig. 1A) in the following referred to as HCHD.[1]

$$C_6H_6 + OH \underset{k_{-1}}{\overset{k_1}{\rightleftharpoons}} HCHD \qquad (R1/-1)$$

Hydrogen abstraction from the aromatic ring by OH radicals is of negligible importance in the atmosphere.[4] At atmospheric O_2 concentrations also unimolecular dissociation (R−1) is negligible because of much faster loss processes for HCHD. In reactions with O_2 the HCHD radical can react irreversibly,

$$HCHD + O_2 \xrightarrow{k_2} \text{products} \qquad (R2)$$

or reversibly to form a peroxy radical, HCHD–O_2 (Fig. 1B):

$$HCHD + O_2 \underset{k_{-3}}{\overset{k_3}{\rightleftharpoons}} HCHD - O_2 \qquad (R3/-3)$$

which can also decompose to other products:

$$HCHD - O_2 \xrightarrow{k_4} \text{products} \qquad (R4)$$

Both, the HCHD radical and HCHD–O_2 interconvert rapidly under atmospheric conditions (k_3 ≈ 1–2 × 10^{-15} cm^3 s^{-1}, $K_{3,-3}$ ≈ 2.5 × 10^{-19} cm^3)[5,6] leading to roughly similar equilibrium concentrations. Because of this fast interconversion, it is difficult to distinguish experimentally between reactions (R2) and (R4). On the other hand, both reactions can form the same products: phenol + HO_2 (Fig. 1C), an epoxide radical (D), or a bicyclic radical (G). D and G are thought to further react with O_2 yielding additional HO_2 plus stable epoxides (E, F) and a bicyclic peroxy radical (H), respectively. The experimentally confirmed main product of these reactions is phenol. The phenol yield of the benzene + OH reaction in air was investigated in several studies

Institut für Energie- und Klimaforschung IEK-8: Troposphäre, Forschungszentrum Jülich GmbH, 52425 Jülich, Germany. E-mail: b.bohn@fz-juelich.de; Fax: +49 2461 615346

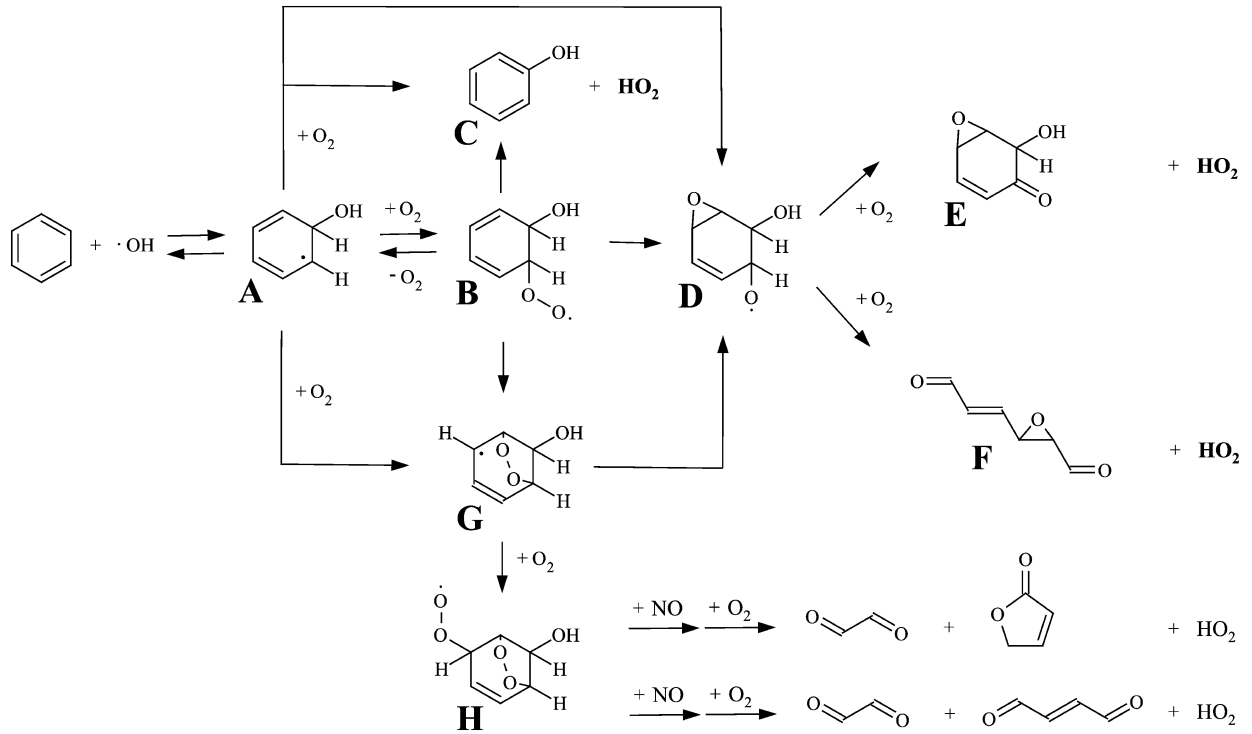

Fig. 1 Currently proposed OH-initiated benzene degradation mechanism.[1,8,9,19,20] For convenience, different resonance structures and possible isomers are not shown. HO_2 formed with no preceding NO reaction is indicated in bold face.

during the last decade[7–11] and the currently proposed value for NO_x free reaction conditions is 0.53 ± 0.07.[12,13] The importance of the reaction pathways forming epoxide products[14] (Fig. 1E and F) is still uncertain. To date, there is no quantitative experimental evidence on the formation of epoxide compounds but species with corresponding molecular weights have been detected.[15–18] An experimentally determined yield of HO_2 formed promptly after the benzene + OH reaction, *i.e.* in the absence of NO, can set a limit to the yield of these epoxides (E, F) and conversely to the yield of the bicyclic peroxy radical (H).

In this article, we describe the first time-resolved detection of OH and HO_2 radicals after pulsed formation of OH in the presence of benzene at variable levels of O_2 using a laser-induced fluorescence (LIF) detection technique. We employed analytical solutions and curve-fitting procedures to derive reaction rate constants and HO_2 yields by comparison to CO reference experiments. CO was chosen as a reference compound because in the presence of O_2 the CO + OH reaction is expected to form HO_2 with unity yield.

2. Experimental

2.1 Setup

The instrument used in this work was originally designed to measure total OH reactivities k_{OH} in ambient air. The total OH reactivity k_{OH} is a pseudo first-order rate constant and given by the following equation:

$$k_{OH} = \sum k_{X_i+OH}[X_i] \quad (1)$$

$[X_i]$ denotes the concentration of a reactive trace constituent and k_{X_i+OH} is the respective second-order rate constant. k_{OH} can be determined by recording decay curves of OH after pulsed formation by laser flash-photolysis. Details on the instrument and its applications can be found elsewhere.[21,22] A scheme of the apparatus is shown in Fig. 2. In this work the setup was used to observe OH and HO_x (= OH + HO_2) decay curves in humidified synthetic air in the presence of selected reactants and traces of ozone produced by O_2 photolysis using a penray lamp. The experiments were performed in a tube-shaped reaction volume under laminar flow conditions at around 298 K and atmospheric pressure. A pulsed laser beam (266 nm, fluence $\sim$1.5 mJ cm^{-2}, pulse duration $\sim$10 ns) from a frequency-quadrupled Nd:YAG laser (Big Sky, CFR200) was passed longitudinally through the tube (shaded area in Fig. 2). Photolysis of O_3 at 266 nm followed by reaction of $O(^1D)$ with water vapour led to virtually instantaneous OH formation. Concentration levels of O_3 and H_2O were about 1×10^{12} cm^{-3} and 3×10^{17} cm^{-3}, respectively, resulting in initial OH concentrations $\leq 5 \times 10^9$ cm^{-3}.

OH radicals were detected 50 cm downstream of the tube inlet by a laser-induced fluorescence technique. Air was sampled from the center of the tube into a low pressure detection cell (350 Pa) through a 0.2 mm nozzle. OH fluorescence at 308 nm was induced with a pulsed, tunable dye laser which was pumped by the 532 nm radiation from a high repetition rate (8.5 kHz) frequency-doubled Nd:YAG laser (Navigator I, Spectra Physics). The fluorescence was detected by gated photon counting and the photon counts were recorded by a multichannel scaler over a 1 s time interval at a resolution of 5 ms. Signal averaging of the decay curves was applied to improve the signal-to-noise ratio. Data from the first 10 ms after the laser flash were discarded because the

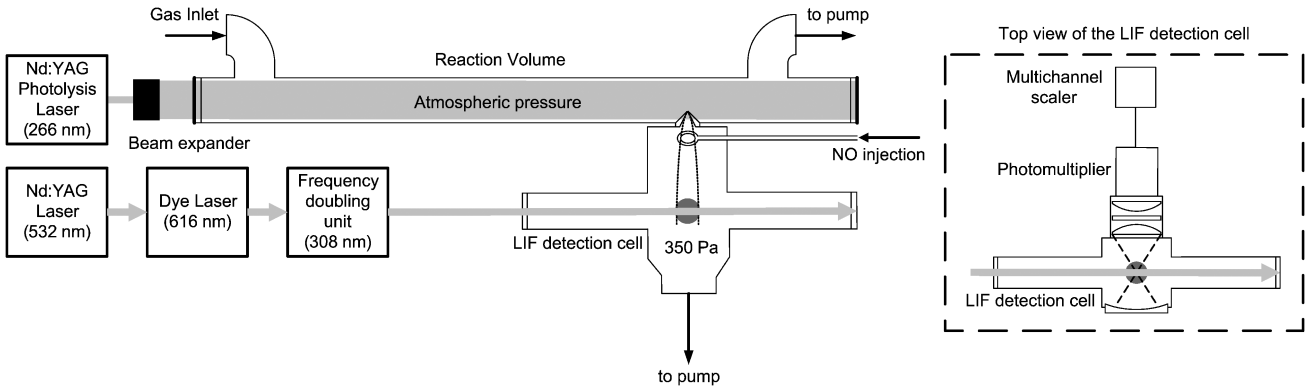

Fig. 2 Scheme of the experimental setup. The shaded area indicates the volume illuminated by the pulsed 266 nm photolysis laser. Time-resolved OH detection is made in a gas expansion in the attached low pressure LIF detection cell.

signal in this interval was very noisy. This was possibly caused by laser profile inhomogeneities or the local influence of the nozzle on the photolysis laser beam, *i.e.* the initial distribution of OH radicals, which is then diminished by the gas flow through the reaction cell.

By adding a small flow of pure NO into the expanding gas upstream of the detection zone, HO_2 can be partly converted to OH and detected as an additional fluorescence signal (HO_x measurement mode).

$$HO_2 + NO \rightarrow OH + NO_2 \qquad (R5)$$

In this work, the NO injection—originally developed to measure atmospheric HO_2 radicals[23,24]—was implemented in the OH reactivity instrument for the first time, in order to alternately measure OH and HO_x. Switching between the measurement modes was possible within a few minutes. To verify that experimental conditions remained constant, OH decays were recorded before and after the HO_x measurements.

In clean N_2/O_2 mixtures with premixed water vapour and ozone, background OH reactivities of $k^0_{OH} = (2.5 \pm 0.3)\ s^{-1}$ were observed that were assigned to diffusion and wall loss. The contribution of the O_3 + OH reaction to the background reactivity was minor ($\sim$0.1 s^{-1}). Experiments were conducted with excess concentrations of reactants, *i.e.* under pseudo first-order conditions at $k_{OH} \approx 20\ s^{-1}$. Numerical simulations showed that radical–radical reactions can be disregarded at the estimated initial OH concentration. The content of the reaction cell was completely changed during the time between photolysis laser shots (2.5 s). Photolysis of reaction products can thus be excluded as source of HO_2 or H-atoms. It has been shown that H atoms are formed in the 248 nm pulsed photolysis of benzene;[25–27] tests in the absence of O_3 showed no detectable OH or H atom formation at 266 nm in the present experiments. The same applies to the other reactants used. The HO_2 background decay rate of $k^0_{HO_2} = (1.7 \pm 0.3)\ s^{-1}$ that was measured upon addition of CO was attributed to diffusion and wall losses. The nature of this loss is secondary for the analysis of this work as long as it resulted in an exponential decay. This was the case within the noise of the data. There was no indication that $k^0_{HO_2}$ changed upon addition of reactants other than CO (*e.g.* benzene).

The LIF detection system exhibits cross-sensitivity to specific RO_2 species as shown in this and another related paper.[28] In general, RO_2 radicals react with NO and form RO radicals:

$$RO_2 + NO \rightarrow RO + NO_2 \qquad (R6)$$

In the case of simple alkoxy radicals (C1–C4), RO reacts with O_2 and forms HO_2 and a carbonyl compound:

$$RO + O_2 \rightarrow R'CHO + HO_2 \qquad (R7)$$

Because of the short reaction time and the reduced O_2 number density in the gas expansion, the formation rate of HO_2 is slow and further conversion into detectable amounts of OH is negligible. However, in the case of RO_2 species resulting from the reaction of OH with alkenes or aromatics, the RO radicals formed in reaction (R6) can undergo fast decomposition followed by rapid formation of HO_2. In this case, a significant amount of HO_2 is converted to OH and detected by LIF.[28] The ratio α_{RO_2} of the detection sensitivities of RO_2 to HO_2 decreases with decreasing NO. Therefore, to quantify and finally avoid the RO_2 interference, the NO concentration in the LIF detection cell was varied over a wide range. In addition to benzene, isoprene and cyclohexane were used as test reactants that were expected to form RO radicals with strongly different behaviour with regard to HO_2 formation in secondary reactions.

2.2 Materials

N_2/O_2 mixtures were made from highly purified (99.9999%) liquid samples of N_2 and O_2. In order to premix water vapour, the gas flow passed a saturator filled with pure water (Milli-Q). Liquid benzene (Merck), cyclohexane (Merck) and isoprene (Aldrich, stabilized by 100 ppm of 4-*tert*-butylbenzene-1,2-diol) had a stated purity of 99.8%, 99.5% and 99%, respectively. Microlitre amounts of the liquids were injected into a silcosteel container and pressurised to 330 kPa with synthetic air. The gas mixture from the silcosteel container was then introduced with a mass flow controller to the main gas flow. The concentration of the respective VOC was estimated from the measured OH reactivity. A 1% mixture of CO in nitrogen was used for experiments, when CO was added (99.997%, Messer Griesheim). Pure NO (99.5%, Linde) used for the conversion of HO_2 to OH in the detection cell passed a cartridge filled with sodium hydroxide coated silicate (Ascerite, Sigma-Aldrich) to remove impurities.

3. Data evaluation

HO_2 yields were extracted from the measured OH and HO_x decay curves in the presence of benzene and other hydrocarbons by comparison to CO reference experiments. The CO + OH reaction gives CO_2 and H atoms. The intermediately formed H atoms react with O_2 to give HO_2 virtually instantaneously on the time scale of the experiment ($k_H \approx 6 \times 10^6\ s^{-1}$ in air).

$$CO + OH \rightarrow CO_2 + H \quad (R8)$$

$$H + O_2 + M \rightarrow HO_2 + M \quad (R9)$$

For the CO experiments, an exponential decay of OH is expected:

$$[OH] = [OH]_0 \times \exp(-k_{OH}^{CO} t) \quad (2)$$

k_{OH}^{CO} is the total OH reactivity in the presence of CO including the background OH reactivity k_{OH}^0.

$$k_{OH}^{CO} = k_{CO+OH}[CO] + k_{OH}^0 \quad (3)$$

For HO_2 the reaction sequence (R8), (R9), followed by a loss of HO_2, results in the following expression:

$$[HO_2] = \frac{[OH]_0 (k_{OH}^{CO} - k_{OH}^0)\phi_{HO_2}^{CO}}{k_{OH}^{CO} - k_{HO_2}^0} \times \{\exp(-k_{HO_2}^0 t) - \exp(-k_{OH}^{CO} t)\} \quad (4)$$

$\phi_{HO_2}^{CO}$ is the HO_2 yield of the CO + OH reaction. $k_{HO_2}^0$ is the background reactivity of HO_2.

Fig. 3(a) shows examples of OH and HO_x decay curves S_{OH} and S_{HO_x} obtained in the presence of CO. S_{OH} depends on instrument sensitivity and is proportional to the OH concentration:

$$S_{OH} \propto [OH] \quad (5)$$

S_{HO_x} is given by the sum of the OH- and the HO_2-signal. However, S_{HO_x} was somewhat lower than expected because upon addition of NO in the LIF detection cell the sensitivity towards OH was lower by a factor of f_{OH} and the sensitivity towards HO_2 was (typically) lower by a factor of f_{HO_2} compared to OH because of an incomplete conversion.

$$S_{HO_x} \propto f_{OH}([OH] + f_{HO_2}[HO_2]) \quad (6)$$

Assuming $\phi_{HO_2}^{CO} = 1$, the fit of the data in Fig. 3(a) gives values of $f_{OH} = 0.91$ and $f_{HO_2} = 0.45$.

Also in the case of the hydrocarbon + OH reactions, the HO_2 formation in a first approach was assumed to be effectively undelayed on the timescale of the experiments:

$$\text{Hydrocarbon} + OH + O_2 \rightarrow HO_2 + \text{other products} \quad (R10)$$

For the benzene experiments in air this assumption is justified because the lifetime of HCHD is much shorter ($k_{HCHD} \approx 500\ s^{-1}$ in air)[5] compared to OH. Again, an exponential expression for the OH concentration,

$$[OH] = [OH]_0 \times \exp(-k_{OH}^{HC} t) \quad (7)$$

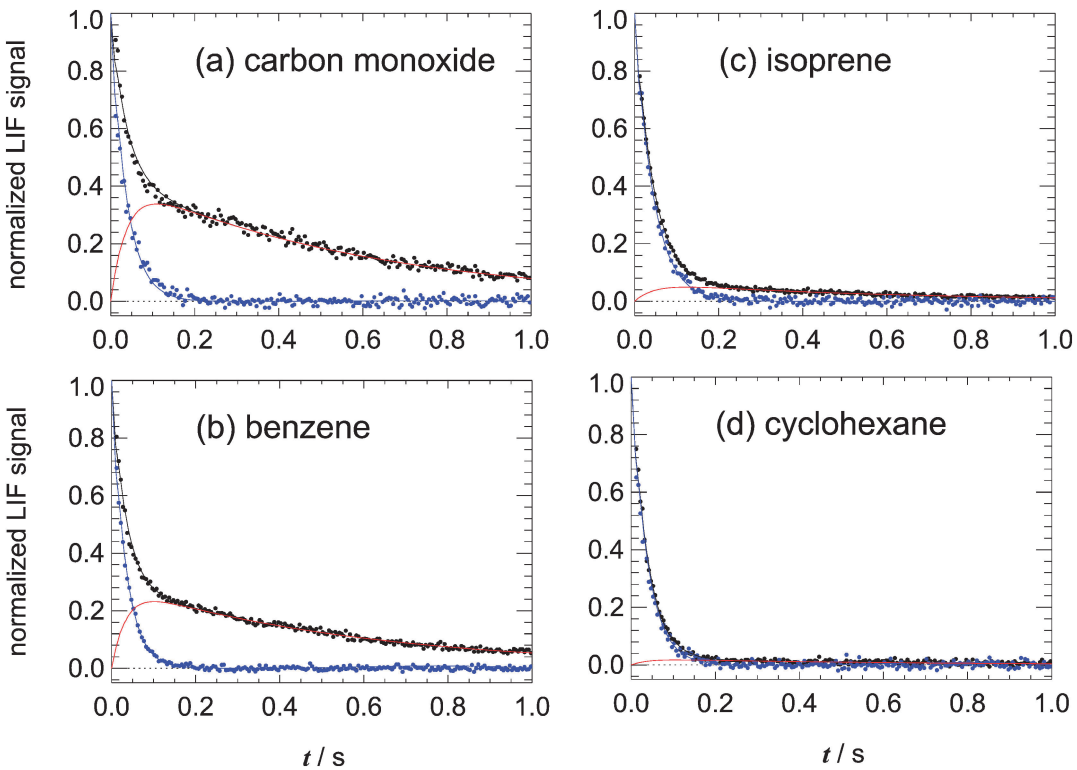

Fig. 3 Normalized S_{OH} (blue points) and S_{HO_x} (black points) obtained in the presence of CO, benzene, isoprene and cyclohexane in synthetic air in the absence of NO in the reaction volume. The NO concentration in the LIF detection cell was $1.2 \times 10^{14}\ cm^{-3}$ in each experiment (see the text). Full lines correspond to fitted decays according to eqn (2), (4), (7) and (8). The red lines show the fitted contributions of HO_2 to S_{HO_x}. (a) is the corresponding reference experiment for (b). For (c) and (d) these experiments are not shown.

and a biexponential expression for the HO_2 concentration were obtained.

$$[HO_2] = \frac{[OH]_0(k_{OH}^{HC} - k_{OH}^0)\phi_{HO_2}^{HC}}{k_{OH}^{HC} - k_{HO_2}^0} \times \{\exp(-k_{HO_2}^0 t) - \exp(-k_{OH}^{HC} t)\} \quad (8)$$

k_{OH}^{HC} is the total OH reactivity in the presence of the hydrocarbon.

$$k_{OH}^{HC} = k_{HC+OH}[HC] + k_{OH}^0 \quad (9)$$

$\phi_{HO_2}^{HC}$ is the yield of HO_2 following the hydrocarbon + OH reaction. This yield should be considered effective because HO_2 formation involves at least two elementary reactions, *i.e.* the initial OH reaction and a succeeding, fast O_2 reaction. In experiments with benzene under conditions with reduced O_2, the lifetime of HCHD increases and a delayed formation of HO_2 is expected, as well as a biexponential decay for OH. Accordingly, more complex formulas were derived for these conditions (see Section 4.2).

Any formation of RO_2 radicals can be treated in a similar way as for HO_2. Assuming $k_{HO_2}^0 = k_{RO_2}^0$ the time dependence of RO_2 radicals is identical to that of HO_2, but with a yield $\phi_{RO_2}^{HC}$ instead of $\phi_{HO_2}^{HC}$. Because of the potential RO_2 interference (eqn (R6) and (R7)), S_{HO_x} may contain an additional term compared to eqn (6):

$$S_{HO_x} \propto f_{OH}([OH] + f_{HO_2}([HO_2] + \alpha_{RO_2}[RO_2])) \quad (10)$$

The additional term can be rearranged to a factor F_{RO_2} utilising the same time-dependencies of HO_2 and RO_2:

$$S_{HO_x} \propto f_{OH}([OH] + f_{HO_2}[HO_2](1 + \alpha_{RO_2}\phi_{RO_2}^{HC}/\phi_{HO_2}^{HC})) = f_{OH}([OH] + f_{HO_2}[HO_2]F_{RO_2}) \quad (11)$$

Thus, also in the presence of RO_2 eqn (8) is applicable except for a factor $F_{RO_2} \geq 1$. F_{RO_2} is expected to approach unity upon decreasing the amount of NO added within the LIF detection cell, *i.e.* for decreasing α_{RO_2}.

To extract the product $\phi_{HO_2}^{HC} F_{RO_2} = \Phi^{HC}$ from the data, the analytical expressions of eqn (2), (4), (7) and (8) were fitted simultaneously to the four S_{OH} and S_{HO_x} decay curves obtained in the presence of CO and the respective hydrocarbon using a Levenberg–Marquardt least squares fitting procedure.[29] Setting $\phi_{HO_2}^{CO} = 1$, the factors f_{OH}, f_{HO_2}, the decay rates k_{OH}^{CO} and k_{OH}^{HC} and Φ^{HC} were determined. The separately measured k_{OH}^0 was held fixed at 2.5 s^{-1}. Fig. 3(a) and (b) show examples of associated measurements with CO and benzene and the corresponding fits.

The fit quality was evaluated from the weighted summed squared residuals χ^2 divided by the degrees of freedom (DOF $\approx$ number of data points) that should range around unity. Fitting the CO and hydrocarbon data together typically resulted in $\chi^2/DOF \approx 1.3$. The deviation from unity is acceptable and indicates that the precisions of the data points that were estimated from Poisson statistics were slightly underestimated. To estimate errors of the fitted Φ^{HC}, it was supposed that values of $\chi^2 \times 1.023$ are still acceptable within the experimental scatter. The factor 1.023 was taken from a parametrization of values for the χ^2-distribution for DOF = 792 to obtain a probability of $\sim$0.68. Φ^{HC} was varied and held fixed during the fits until this quality level was reached. The resulting ranges correspond to estimated 1σ errors.

4. Results

4.1 Benzene + OH reaction in synthetic air and interferences from peroxy radicals

Table 1 gives a summary of fitted Φ^{HC} and other parameters obtained in synthetic air with the reactants benzene, isoprene and cyclohexane at different NO concentrations in the LIF detection cell. This NO concentration will be denoted as $[NO]_D$ in the following to emphasise that it applies to the detection cell and not to the main reaction volume where no NO was present. The data of Table 1 are also plotted in Fig. 4 as a function of $[NO]_D$. For benzene and isoprene the dependence of Φ^{HC} on $[NO]_D$ hints towards a significant contribution of interferences caused by the presence of peroxy radicals. Thus, the limiting values of Φ^{HC} towards low $[NO]_D$ are the $\phi_{HO_2}^{HC}$ under consideration.

Table 1 Fit results of combined CO/hydrocarbon experiments in synthetic air at different NO concentrations in the LIF detection cell, $[NO]_D$. Results were obtained by fitting eqn (2), (4), (7) and (8) to the S_{OH} and S_{HO_x} **decay curves**

Reactant	$[NO]_D/10^{15}$ cm^{-3}	f_{OH}	f_{HO_2}	$\Phi^{HC} = \phi_{HO_2}^{HC} F_{RO_2}$	χ^2/DOF
Benzene	0.04	0.85	0.23	0.69 ± 0.10	1.09
	0.12	0.91	0.45	0.67 ± 0.08	1.30
	0.39	0.86	0.75	0.77 ± 0.10	1.24
	0.66	0.81	0.96	0.84 ± 0.09	1.19
	1.50	0.82	1.36	0.81 ± 0.09	1.30
	2.37	0.73	1.63	0.81 ± 0.08	1.21
	3.03	0.80	1.61	0.87 ± 0.08	1.57
Isoprene	0.04	0.86	0.23	0.11 ± 0.04	1.15
	0.12	0.92	0.45	0.15 ± 0.02	1.25
	0.39	0.87	0.75	0.30 ± 0.04	1.26
	0.66	0.77	0.98	0.44 ± 0.06	1.33
	1.50	0.79	1.39	0.69 ± 0.10	1.62
	2.37	0.73	1.63	0.93 ± 0.15	1.86
	3.03	0.79	1.62	0.96 ± 0.11	2.15
Cyclohexane	0.12	0.94	0.53	0.04 ± 0.02	1.22
	3.03	0.86	1.50	0.11 ± 0.02	1.74

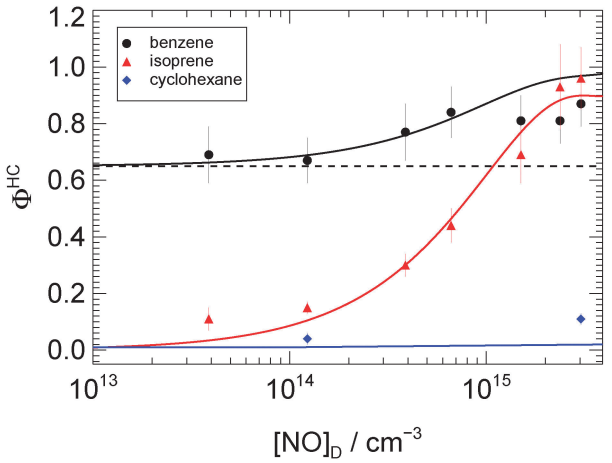

Fig. 4 Dependence of fitted Φ^{HC} on $[NO]_D$, the NO concentration in the LIF detection cell. Symbols show results of combined CO/hydrocarbon experiments (black: benzene, red: isoprene, blue: cyclohexane). The solid lines show the simulated $[NO]_D$ dependence of Φ^{HC} based on the reactions in Table 2. The dashed black line indicates the presumed contribution of $\phi_{HO_2}^{benzene}$ to $\Phi^{benzene}$ following the benzene + OH reaction.

To reproduce the increase of Φ^{HC} with $[NO]_D$, we applied a numerical model for the reactions within the detection cell. The model runs are based on an estimated reaction time of 250 μs, a total pressure of 350 Pa, a temperature of 298 K and the assumption of ideal mixing of added NO. The reaction time was obtained by fitting the increase of f_{HO_2} with $[NO]_D$ taking into account the reactions OH + NO and HO_2 + NO and an extra factor allowing for maximum values $f_{HO_2} > 1$ as found experimentally. The latter can be rationalised by greater losses of OH at the nozzle compared to HO_2. Because ideal mixing of NO cannot be verified, the actually fitted quantity is the product of effective NO concentration and reaction time but that should work similarly on HO_2 and RO_2. More details on these aspects, as well as the influence of temperature and nozzle size are given elsewhere.[28]

The full lines in Fig. 4 show the ratios of calculated OH concentrations obtained for the different hydrocarbons compared with a reference case where pure HO_2 was entering the detection cell. Table 2 gives an overview of the relevant reactions for the three hydrocarbons investigated here. For benzene an initial ϕ_{RO_2}/ϕ_{HO_2} ratio of 0.35/0.65 was assumed,[13,36] while for isoprene and cyclohexane the model started with pure RO_2.[2]

In the case of benzene, the Φ^{HC} showed a slight dependence on $[NO]_D$. The increase at elevated $[NO]_D$ was assigned to subsequent reactions of the bicyclic peroxy radicals (Fig. 1H). The calculations quantifying the RO_2 conversion efficiency are in good agreement with the experimental results. While at $[NO]_D$ exceeding 10^{15} cm^{-3} the model slightly over-predicts Φ^{HC}, the behaviour towards low $[NO]_D$ is in excellent agreement with the measurements. The absolute agreement is fortunate but the model calculations also indicate that the limiting value was already reached in good approximation at $[NO]_D \leq 1.2 \times 10^{14}$ cm^{-3}, *i.e.* $\Phi^{HC} = \phi_{HO_2}^{benzene}$. Thus, $\phi_{HO_2}^{benzene} = 0.69 \pm 0.10$ is the HO_2 yield following the OH + benzene reaction in synthetic air. A further reduction of $[NO]_D$ was not useful since it resulted in HO_2 sensitivity factors of $f_{HO_2} \leq 0.24$, so that S_{OH} and S_{HO_x} hardly differed.

To ensure that the limiting behaviour was reproduced correctly by the model, the measurements with isoprene were consulted for comparison. The isoprene + OH reaction was assumed to produce peroxy radicals with about unity yield in synthetic air but no HO_2.[2] The subsequent chemistry of these radicals in the presence of NO is expected to rapidly form HO_2 at a rate comparable to that of peroxy radicals (H) from benzene. In both cases the intermediately formed alkoxy radicals quickly decompose with an estimated rate constant of 10^6 s^{-1} (see Table 2). The radical products of these decompositions, HC(O)–CH–OH and CH_2–OH, rapidly react with O_2 to form HO_2 + glyoxal and HO_2 + formaldehyde, respectively. The experimentally obtained Φ^{HC} in the case of isoprene indeed showed a consistent dependence on $[NO]_D$ with a value approaching zero in good approximation at low $[NO]_D$. The minimum value of 0.11 ± 0.04 obtained at the lowest $[NO]_D$ could hint towards a minor, direct HO_2 formation with an upper limit $\phi_{HO_2}^{isoprene} \leq 0.10$. On the other hand, a residual interference from peroxy radicals not accounted for in the model calculations can also not be excluded considering the assumptions mentioned above (reaction time, NO mixing behaviour and temperature).

Cyclohexane was chosen as a further test reactant, since the secondary chemistry of peroxy radicals from OH + cyclohexane in the presence of NO was expected to form HO_2 significantly slower compared to that of isoprene because of a much slower RO + O_2 reaction with no preceding RO decomposition (see Table 2). In accordance with that, the observed Φ^{HC} were very small and hardly increased with $[NO]_D$, although calculations slightly underpredict the observed values. Again, this can be explained by an upper limit $\phi_{HO_2}^{cyclohexane} \leq 0.05$ or model deficiencies underestimating RO_2 interferences.

4.2 Benzene + OH reaction at low O_2 concentration

In addition to the experiments in synthetic air, we investigated the secondary HO_2 formation following the benzene + OH reaction at reduced O_2 concentrations. $[NO]_D$ was kept low at 1.2×10^{14} cm^{-3} to avoid any RO_2 interference. Under conditions with low O_2, a delayed formation of HO_2 was expected. The question was if the HO_2 yields are similar and if the rate constant of HCHD + O_2 can be determined. As was shown previously, the existence of the equilibrium (R3, −3) does not influence the HCHD + O_2 kinetics at low O_2. Regardless of the actual mechanism, possibly involving reactions (R2), (R3, −3) and (R4), the HCHD loss is correctly described by an effective second-order rate constant $k'_2 = k_2 + K_3 k_4$.[5]

Two test experiments at different O_2 concentrations were made to determine k'_2 and the HO_2 yields. However, it turned out that the results were inconsistent with O_2 being the only reactant forming HO_2. A further experiment at increased O_3 concentration revealed that also the reaction

$$\text{HCHD} + \text{O}_3 \xrightarrow{k_{11}} \text{products} \qquad \text{(R11)}$$

significantly contributed to the HCHD loss rate constant and to secondary formation of HO_2.

Table 2 Relevant reactions and reaction rate constants for radical conversions in the LIF detection cell to model interferences from peroxy radicals. Rate constants are calculated for a temperature of 298 K

Reaction	k		
$HO_2 + NO \rightarrow OH + NO_2$	8.1×10^{-12} cm^3 s^{-1} [a]		
$OH + NO \rightarrow HONO$	5.7×10^{-14} cm^3 s^{-1} [a,b]		
$OH + NO_2 \rightarrow HNO_3$	1.4×10^{-13} cm^3 s^{-1} [a,b]		
	Benzene	Isoprene	Cyclohexane
$RO_2 + NO \rightarrow RNO_3$	6.8×10^{-13} cm^3 s^{-1} [c]	8.5×10^{-13} cm^3 s^{-1} [c]	6.6×10^{-13} cm^3 s^{-1} [c]
$RO_2 + NO \rightarrow RO + NO_2$	7.8×10^{-12} cm^3 s^{-1} [c]	7.7×10^{-12} cm^3 s^{-1} [c]	7.8×10^{-12} cm^3 s^{-1} [c]
$RO \rightarrow$ fragments	1×10^6 s^{-1} [d]	1×10^6 s^{-1} [e]	—
RO, fragments $+ O_2 \rightarrow HO_2$	9.1×10^{-12} cm^3 s^{-1} [f]	9.1×10^{-12} cm^3 s^{-1} [g]	7.7×10^{-15} cm^3 s^{-1} [h]

[a] NASA recommendation.[30] [b] Calculated for a total pressure of 350 Pa. [c] MCM recommendations[31] based on values for C3–C5 alkyl peroxy radicals.[32–35] [d] MCM recommendation[31] for RO $\rightarrow$ $C_4H_4O_2 + C_2H_3O_2$. $C_4H_4O_2$ represents 2-butenedial and 2(5H)-furanone formed with a branching ratio of 0.5 each, $C_2H_3O_2$ is a radical.[f] [e] MCM recommendation[31] for RO $\rightarrow$ products + CH_2OH (assumed main reaction). [f] $C_2H_3O_2 + O_2 \rightarrow$ glyoxal + HO_2, rate constant assumed similar to $CH_2OH + O_2$. [g] NASA recommendation[30] for $CH_2OH + O_2 \rightarrow HCHO + HO_2$. [h] MCM recommendation[31] for RO $+ O_2 \rightarrow$ cyclohexanone + HO_2.

Fig. 5 shows a semilogarithmic comparison of OH and HO_x decay curves obtained in synthetic air and at a low O_2 concentration ($[O_2] \approx 1.4 \times 10^{16}$ cm^{-3}). The most obvious difference is evident for the OH decays which became biexponential because dissociation of HCHD back to OH + benzene was no longer negligible at low O_2. The following expressions were derived in the literature for the general time-dependencies of OH and HCHD under such quasi-equilibrium conditions:[37,38]

$$[OH] = [OH]_0 \times \left\{ \frac{k_{OH}^{benzene} - \tau_2^{-1}}{\tau_1^{-1} - \tau_2^{-1}} \exp(-\tau_1^{-1} t) + \frac{\tau_1^{-1} - k_{OH}^{benzene}}{\tau_1^{-1} - \tau_2^{-1}} \exp(-\tau_2^{-1} t) \right\} \quad (12)$$

$$[HCHD] = \frac{[OH]_0 (k_{OH}^{benzene} - k_{OH}^0)}{\tau_2^{-1} - \tau_1^{-1}} \times \{\exp(-\tau_1^{-1} t) - \exp(-\tau_2^{-1} t)\} \quad (13)$$

A unity yield of HCHD in reaction (R1) was assumed here. The decay rate coefficients τ_1^{-1} and τ_2^{-1} are given by:

$$\tau_{1,2}^{-1} = \frac{k_{OH}^{benzene} + k_{HCHD}}{2} \pm \sqrt{\left(\frac{k_{OH}^{benzene} - k_{HCHD}}{2}\right)^2 + (k_{OH}^{benzene} - k_{OH}^0) k_{-1}} \quad (14)$$

k_{HCHD} is the total loss rate coefficient for the HCHD intermediate, in this case:

$$k_{HCHD} = k_2'[O_2] + k_{11}[O_3] + k_{-1} + k_{HCHD}^0 = k_R + k_{-1} + k_{HCHD}^0 \quad (15)$$

Because in single experiments no distinction can be made between the contributions of reactions (R2) and (R11), a total rate constant k_R was introduced. For HO_2 the following differential equation was supposed to apply:

$$\frac{d[HO_2]}{dt} = (\phi_{HO_2}^{R2} k_2'[O_2] + \phi_{HO_2}^{R11} k_{11}[O_3])[HCHD] - k_{HO_2}^0 [HO_2] = k_R \phi_{HO_2}^R [HCHD] - k_{HO_2}^0 [HO_2] \quad (16)$$

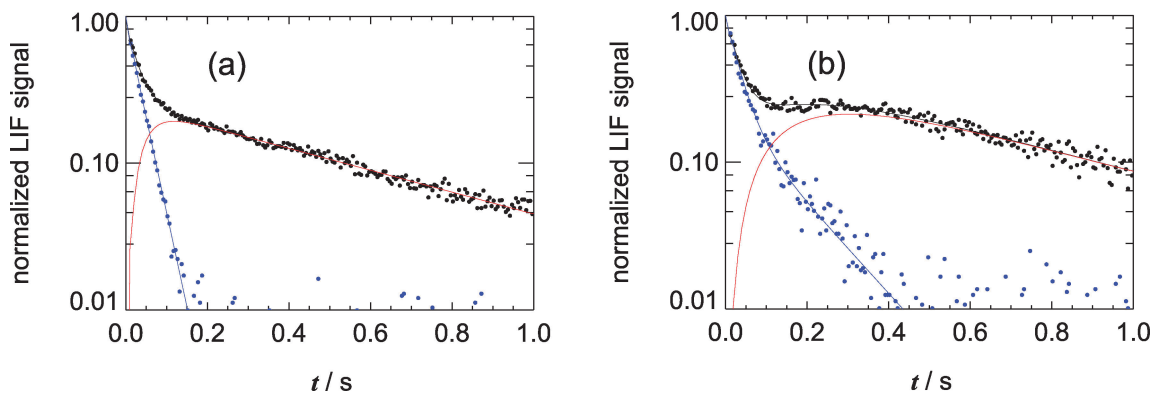

Fig. 5 Semilogarithmic plot of normalized S_{OH} (blue points) and S_{HO_x} (black points) obtained in the presence of benzene. Decay curves were recorded at O_2 concentrations of 5.2×10^{18} cm^{-3} (panel a) and 1.4×10^{16} cm^{-3} (panel b), respectively. The NO concentration in the LIF detection cell was 1.2×10^{14} cm^{-3} in each experiment. Full lines correspond to fitted decays according to eqn (2), (4), (7), and (8) for (a) and accordingly (12) and (18) for (b). The red lines show the fitted contributions of HO_2 to S_{HO_x}.

In the second term an effective HO_2 yield from reactions (R2) and (R11) was defined:

$$\phi^{R}_{HO_2} = \frac{\phi^{R2}_{HO_2} k'_2 [O_2] + \phi^{R11}_{HO_2} k_{11} [O_3]}{k_R} \qquad (17)$$

Inserting [HCHD] from eqn (13) and setting $[HO_2]_0 = 0$ eqn (16) was solved:

$$[HO_2] = \frac{[OH]_0 (k^{benzene}_{OH} - k^0_{OH}) k_R \phi^{R}_{HO_2}}{\tau_1^{-1} - \tau_2^{-1}} \times \left\{ \frac{\exp(-k^0_{HO_2} t)}{k^0_{HO_2} - \tau_1^{-1}} - \frac{\exp(-\tau_1^{-1} t)}{k^0_{HO_2} - \tau_1^{-1}} + \frac{\exp(-\tau_2^{-1} t)}{k^0_{HO_2} - \tau_2^{-1}} - \frac{\exp(-k^0_{HO_2} t)}{k^0_{HO_2} - \tau_2^{-1}} \right\} \qquad (18)$$

In order to analyse the experimental data, the analytical expressions of eqn (2), (4), (12) and (18) were again fitted simultaneously to four S_{OH} and S_{HO_x} decay curves obtained in the presence of CO and benzene. CO experiments at low O_2 were treated like those in synthetic air, because the lifetime of the intermediately formed H-atoms was still negligible ($k_H \approx 15\,000\ s^{-1}$). Besides $\phi^{R}_{HO_2}$ and k_R, two more parameters were fitted: the rate constant of HCHD decomposition k_{-1} and the HCHD background loss rate constant k^0_{HCHD}. The fit results for the three experiments are listed in Table 3. The 1σ errors were assessed as described in Section 3. Mean errors were listed when upper and lower limits were different. The relatively large errors reflect the strong mutual dependencies of fit parameters.

Within the errors the parameters k_{-1} and k^0_{HCHD} are the same in all experiments. In experiment (I) where k_{HCHD} was at a minimum, k_{-1} was determined with the greatest accuracy to be $(3.9 \pm 1.3)\ s^{-1}$. k^0_{HCHD} ranged around $(1.5 \pm 0.2)\ s^{-1}$ in all experiments. To estimate the rate constants k'_2 and k_{11}, the differences in k_R of experiments I and II and experiments I and III were calculated and divided by the differences in O_2 and O_3 concentrations, respectively. This led to $k'_2 = (2.4 \pm 1.1) \times 10^{-16}\ cm^3\ s^{-1}$ and $k_{11} = (5.6 \pm 1.1) \times 10^{-12}\ cm^3\ s^{-1}$. Because the $\phi^{R}_{HO_2}$ showed no difference upon increasing O_2 or O_3, a calculation of the individual HO_2 yields of reactions (R2) and (R11) was not feasible. Within the error limits the effective yields in all three experiments are the same and very close to that obtained in synthetic air. Thus, O_2 and O_3 seem to behave similarly with regard to HO_2 formation, except for the strongly different rate constant.

5. Discussion

In the experiments described above, an HO_2 yield of $\phi^{benzene}_{HO_2} = 0.69 \pm 0.10$ was obtained following the OH + benzene reaction in synthetic air in the absence of NO. This yield is similar to a phenol yield of 0.53 ± 0.07 determined in chamber experiments[8] and to phenol yields determined in flow-tube experiments of 0.61 ± 0.07[10] and 0.51 ± 0.04.[11] Because HO_2 is the expected co-product of phenol formation, this result is consistent with the currently proposed mechanism. Moreover, the remainder $1 - \phi^{benzene}_{HO_2} = 0.31 \pm 0.10$ corresponds very well to an observed yield of glyoxal of 0.35 ± 0.10 from chamber experiments by Volkamer *et al.*[36] under low NO_x conditions and a glyoxal yield of 0.29 ± 0.10 by Berndt and Böge[10] from flow-tube experiments in the presence of NO. Glyoxal is a secondary product of the proposed bicyclic peroxy radical H upon reaction with NO (Fig. 1) and thus HO_2 is not a co-product associated with glyoxal.

On the other hand, based on the data of Volkamer *et al.*,[8,36] Bloss *et al.*[13] determined a yield of epoxides E and F (Fig. 1) of 0.12, in order to close the budget for the OH-initiated degradation of benzene. Taking the data by Berndt and Böge,[10] a similar yield of about 0.10 is obtained. Because formation of epoxides is also associated with HO_2 formation with no preceding NO reaction, the approach by Bloss *et al.*[13] is in accordance with the results of this work. However, given the errors of $\phi^{benzene}_{HO_2}$ we interpret our result merely as a hint towards a minor, but potentially significant (>10%) epoxide formation. A direct, quantitative detection of these species is needed to clarify this point. The experimental method used here could nevertheless help to reduce budget uncertainties for other aromatic compounds. Examples are the xylene and trimethylbenzene isomers where formation of phenolic compounds is of less importance and the yields of epoxides estimated by Bloss *et al.*[13] range between 0.15 and 0.30. Accordingly, for these compounds the HO_2 yield should be significantly greater than the yield of the corresponding phenolic compounds.

At low O_2 concentration, the obtained secondary HO_2 yield was the same as in synthetic air. Despite the potentially complex mechanism of HO_2 formation involving reactions (R2), (R3/−3) and (R4), the ratio of products formed in (R2) and (R4) should be independent of the O_2 concentration. This is in line with the experimental result. The additional rate constants extracted from the decay curves at low O_2 are in good agreement with literature data. Knispel *et al.*,[39] Bohn and Zetzsch,[5] and Raoult *et al.*[6] consistently reported values of k'_2 of (1.6 ± 0.6), (2.1 ± 0.2) and $(2.5 \pm 0.4) \times 10^{-16}\ cm^3\ s^{-1}$ around room temperature. Also the rate constant of HCHD decomposition is in good agreement with available literature

Table 3 Fit results of combined CO/benzene experiments at low O_2 concentrations. Results were obtained by fitting eqn (2), (4), (12) and (18) to the S_{OH} and S_{HO_x} **decay curves. The NO concentration in the LIF detection cell was $[NO]_D = 1.2 \times 10^{14}\ cm^{-3}$. Errors are means of upper and lower limits**

Experiment	$O_2/10^{16}\ cm^{-3}$	$O_3/10^{12}\ cm^{-3}$	k^0_{HCHD}/s^{-1}	k_{-1}/s^{-1}	k_R/s^{-1}	$\phi^{R}_{HO_2}$	χ^2/DOF
I	1.4	0.86	1.6 ± 0.2	3.9 ± 1.3	6.6 ± 1.5	0.83 ± 0.22	1.19
II	3.5	0.86	1.5 ± 0.2	4.9 ± 3.4	11.6 ± 3.9	0.68 ± 0.18	1.22
III	1.4	2.09	1.5 ± 0.1	5.4 ± 2.3	13.5 ± 2.8	0.67 ± 0.12	1.36

data by Wahner and Zetzsch,[37] Witte *et al.*[38] and Knispel *et al.*[39] that range around 3–4 s^{-1}.

The situation at low O_2 was complicated by the unexpected influence of the HCHD + O_3 reaction. So far no rate constant has been reported for this reaction which is much faster than the O_2 reaction but slower by a factor of about five compared to the HCHD + NO_2 reaction.[40] The HO_2 yield of the HCHD + O_3 reaction is apparently similar to that of the O_2 reaction. Possible co-products of HO_2 are benzene and O_2:

$$\text{HCHD} + O_3 \rightarrow HO_2 + O_2 + \text{benzene} \qquad \text{(R12)}$$

No evidence was found for the formation of OH, *e.g. via*

$$\text{HCHD} + O_3 \rightarrow OH + O_2 + \text{phenol} \qquad \text{(R13)}$$

because that would have led to an apparent increase of the rate constant k_{-1}. However, given the errors of the fitted parameters this reaction cannot be ruled out completely. Overall, the HCHD + O_3 reaction is not expected to be of relevance in the atmosphere because of the dominating role of O_2 despite the small rate constant of the HCHD + O_2 reaction.

It should be noted that also for OH + isoprene reaction in air a direct formation of HO_2 from peroxy radicals was postulated in the recent literature,[41,42] with rate constants ranging from 0.1 s^{-1} to 8 s^{-1}. Except for the upper limit for a fast HO_2 formation determined above, we can exclude a significant ($\geq 10\%$) formation of HO_2 with a rate constant $\geq 0.5\ s^{-1}$. Smaller rate constants were beyond the scope of the current apparatus.

The results regarding the secondary HO_2 yields discussed above were obtained under conditions where interferences of the HO_2 detection by peroxy radicals were estimated negligible based on the characterisation of the instrument shown in Fig. 4. When this study began we were not aware of the importance of these interferences for an accurate measurement of HO_2 by the LIF method. This also applies for measurements of atmospheric HO_2. The implications go far beyond the scope of this study and stimulated extensive tests with a number of hydrocarbons using an instrument dedicated for atmospheric HO_x measurements. The results are reported in a separate paper by Fuchs *et al.*[28] Moreover, the effects on the analysis of existing data sets from recent field measurements are accounted for in a further publication by Lu *et al.*[43]

Despite these problems, radical detection by LIF in a gas expansion applied in this work has several advantages for kinetic experiments. Firstly, in contrast to classical OH detection schemes *via* resonance fluorescence or laser-induced fluorescence, OH can be detected at atmospheric pressure and O_2 levels because the gas expansion strongly reduces fluorescence quenching. Secondly, the sensitivity is great enough to obtain high quality OH decay curves at OH starting concentrations where radical–radical reactions can be neglected in good approximation. Thirdly, the possibility of an associated detection of HO_2 at such low radical concentrations is an option that has so far not been utilised for kinetic experiments.

6. Conclusions

In this work a direct formation of HO_2 following the OH + benzene reaction in synthetic air in the absence of NO was observed for the first time. Interferences of the HO_2 LIF detection method in the presence of peroxy radicals were quantified and avoided by reducing the necessary NO addition within the LIF detection cell. The HO_2 yield was determined to be 0.69 ± 0.10 in accordance with currently proposed mechanisms for the OH-initiated benzene degradation. By comparison with phenol yields from the recent literature, a minor ~10% formation of other HO_2 co-products, *e.g.* epoxides, is possible within the error limits. Measurements at low O_2 concentration (0.06–0.14% in N_2) gave similar HO_2 yields and rate constants for the benzene–OH adduct reactions with O_3 and O_2, and the thermal decomposition of the adduct back to OH + benzene. The latter two rate constants are in good agreement with the literature, the rate constant of $(5.6 \pm 1.1) \times 10^{-12}$ $cm^3\ s^{-1}$ for the adduct + O_3 reaction was not reported before.

Acknowledgements

The authors thank F. Rohrer, F. Holland, S. Lou and M. Bachner for useful discussions and technical support. S. Nehr thanks the Deutsche Forschungsgemeinschaft for PhD studentship funding under grant BO 1580/3-1.

References

1 J. G. Calvert, R. Atkinson, K. H. Becker, R. M. Kamens, J. H. Seinfeld, T. J. Wallington and G. Yarwood, *Mechanisms of atmospheric oxidation of aromatic hydrocarbons*, Oxford University Press, 2002.
2 R. Atkinson and J. Arey, *Chem. Rev.*, 2003, **103**, 4605–4638.
3 T. J. Fortin, B. J. Howard, D. D. Parrish, P. D. Goldan, W. C. Kuster, E. L. Atlas and R. A. Harley, *Environ. Sci. Technol.*, 2005, **39**, 1403–1408.
4 R. Atkinson, *J. Phys. Chem. Ref. Data*, 1989, **Monograph 1**, 204.
5 B. Bohn and C. Zetzsch, *Phys. Chem. Chem. Phys.*, 1999, **1**, 5097–5107.
6 S. Raoult, M. T. Rayez, J. C. Rayez and R. Lesclaux, *Phys. Chem. Chem. Phys.*, 2004, **6**, 2245–2253.
7 T. Berndt and O. Böge, *Int. J. Chem. Kinet.*, 2001, **33**, 124–129.
8 R. Volkamer, B. Klotz, I. Barnes, T. Imamura, K. Wirtz, N. Washida, K. H. Becker and U. Platt, *Phys. Chem. Chem. Phys.*, 2002, **4**, 1598–1610.
9 B. Klotz, R. Volkamer, M. D. Hurley, M. P. S. Andersen, O. J. Nielsen, I. Barnes, T. Imamura, K. Wirtz, K. H. Becker, U. Platt, T. J. Wallington and N. Washida, *Phys. Chem. Chem. Phys.*, 2002, **4**, 4399–4411.
10 T. Berndt and O. Böge, *Phys. Chem. Chem. Phys.*, 2006, **8**, 1205–1214.
11 J. Noda, R. Volkamer and M. J. Molina, *J. Phys. Chem. A*, 2009, **113**, 9658–9666.
12 C. Bloss, V. Wagner, A. Bonzanini, M. E. Jenkin, K. Wirtz, M. Martin-Reviejo and M. J. Pilling, *Atmos. Chem. Phys.*, 2005, **5**, 623–639.
13 C. Bloss, V. Wagner, M. E. Jenkin, R. Volkamer, W. J. Bloss, J. D. Lee, D. E. Heard, K. Wirtz, M. Martin-Reviejo, G. Rea, J. C. Wenger and M. J. Pilling, *Atmos. Chem. Phys.*, 2005, **5**, 641–664.
14 L. Bartolotti and E. Edney, *Chem. Phys. Lett.*, 1995, **245**, 119–122.
15 J. Z. Yu, H. E. Jeffries and K. G. Sexton, *Atmos. Environ.*, 1997, **31**, 2261–2280.
16 J. Z. Yu and H. E. Jeffries, *Atmos. Environ.*, 1997, **31**, 2281–2287.

17 E. S. C. Kwok, S. M. Aschmann, R. Atkinson and J. Arey, *J. Chem. Soc., Faraday Trans.*, 1997, **93**, 2847–2854.
18 J. Zhao, R. Zhang, K. Misawa and K. Shibuya, *J. Photochem. Photobiol., A*, 2005, **176**, 199–207.
19 T. H. Lay, J. W. Bozzelli and J. H. Seinfeld, *J. Phys. Chem.*, 1996, **100**, 6543–6554.
20 T. Berndt and O. Böge, *Phys. Chem. Chem. Phys.*, 2001, **3**, 4946–4956.
21 A. Hofzumahaus, F. Rohrer, K. Lu, B. Bohn, T. Brauers, C.-C. Chang, H. Fuchs, F. Holland, K. Kita, Y. Kondo, X. Li, S. Lou, M. Shao, L. Zeng, A. Wahner and Y. Zhang, *Science*, 2009, **324**, 1702–1704.
22 S. Lou, F. Holland, F. Rohrer, K. Lu, B. Bohn, T. Brauers, C. Chang, H. Fuchs, R. Häseler, K. Kita, Y. Kondo, X. Li, M. Shao, L. Zeng, A. Wahner, Y. Zhang, W. Wang and A. Hofzumahaus, *Atmos. Chem. Phys.*, 2010, **10**, 11243–11260.
23 F. Holland, U. Aschmutat, M. Hessling, A. Hofzumahaus and D.-H. Ehhalt, *J. Atmos. Chem.*, 1998, **31**, 205–225.
24 F. Holland, A. Hofzumahaus, R. Schäfer, A. Kraus and H.-W. Pätz, *J. Geophys. Res., [Atmos.]*, 2003, **108**, 8246–8268.
25 A. Aluculesei, A. Tomas, C. Schoemaecker and C. Fittschen, *Appl. Phys. B: Lasers Opt.*, 2008, **92**, 379–385.
26 T. Kovacs, M. A. Blitz, P. W. Seakins and M. J. Pilling, *J. Chem. Phys.*, 2009, **131**, 204304.
27 C. Jain, A. E. Parker, C. Schoemaecker and C. Fittschen, *ChemPhysChem*, 2010, **11**, 3867–3873.
28 H. Fuchs, B. Bohn, A. Hofzumahaus, F. Holland, K. D. Lu, S. Nehr, F. Rohrer and A. Wahner, *Atmos. Meas. Tech. Discuss.*, 2011, **4**, 1255–1302.
29 Craig Markwardt, IDL Library, http://cow.physics.wisc.edu/~craigm/idl/, 2010.
30 NASA panel for data evaluation, JPL publication, 2010, 09-31, evaluation NO. 16.
31 MCM, Master Chemical Mechanism, http://mcm.leeds.ac.uk/MCM/, 2011.
32 W. Carter and R. Atkinson, *J. Atmos. Chem.*, 1989, **8**, 165–173.
33 J. Eberhard and C. Howard, *Int. J. Chem. Kinet.*, 1996, **28**, 731–740.
34 J. Eberhard and C. Howard, *J. Phys. Chem. A*, 1997, **101**, 3360–3366.
35 R. Atkinson, D. Baulch, R. Cox, R. Hampson, J. Kerr, M. Rossi and J. Troe, IUPAC Subcommittee Gas Kinetic Data Evaluation, *J. Phys. Chem. Ref. Data*, 1999, **28**, 191–393.
36 R. Volkamer, U. Platt and K. Wirtz, *J. Phys. Chem. A*, 2001, **105**, 7865–7874.
37 A. Wahner and C. Zetzsch, *J. Phys. Chem.*, 1983, **87**, 4945–4951.
38 F. Witte, E. Urbanik and C. Zetzsch, *J. Phys. Chem.*, 1986, **90**, 3251–3259.
39 R. Knispel, R. Koch, M. Siese and C. Zetzsch, *Ber. Bunsen-Ges.*, 1990, **94**, 1375–1379.
40 R. Koch, R. Knispel, M. Elend, M. Siese and C. Zetzsch, *Atmos. Chem. Phys.*, 2007, **7**, 2057–2071.
41 J. Peeters, T. L. Nguyen and L. Vereecken, *Phys. Chem. Chem. Phys.*, 2009, **11**, 5935–5939.
42 J. Peeters and J.-F. Müller, *Phys. Chem. Chem. Phys.*, 2010, **12**, 14227–14235.
43 K. D. Lu, F. Rohrer, F. Holland, H. Fuchs, B. Bohn, T. Brauers, C. C. Chang, R. Häseler, M. Hu, K. Kita, Y. Kondo, X. Li, S. R. Lou, S. Nehr, M. Shao, L. M. Zeng, A. Wahner, Y. H. Zhang and A. Hofzumahaus, *Atmos. Chem. Phys. Discuss.*, 2011, **11**, 11311–11378.